On the tidal dependence of galaxy properties

Heling Yan[1*], Zuhui Fan[1] and Simon D. M. White[2]

[1]*Department of Astronomy, Peking University, YiHeYuan-Road 5, 100871 Beijing, China*
[2]*Max Planck Institute for Astrophysics, Karl-Schwarzschild-Strasse 1, 85740 Garching, Germany*

25 February 2013

ABSTRACT
Using volume-limited samples drawn from The Sloan Digital Sky Survey Data Release 7 (SDSS DR7), we measure the tidal environment of galaxies, which we characterize by the ellipticity e of the potential field calculated from the smoothed spatial number density $1 + \delta$ of galaxies. We analyze if galaxy properties, including color, $D_n 4000$, concentration and size correlate with e, in addition to depending on $1 + \delta$. We find that there exists a transition smoothing scale at which correlations/anti-correlations with e reverse. This transition scale is well represented by the distance to the 3rd-nearest-neighbor of a galaxy in a volume limited sample with $M_r < -20$ which has a distribution peaked at $\sim 2\ h^{-1}$Mpc. We further demonstrate that this scale corresponds to that where the correlation between the color of galaxies and environmental density $1+\delta$ is the strongest. For this optimal smoothing R_0 no additional correlations with e are observed. The apparent dependence on tidal ellipticity e at other smoothing scales R_s can be viewed as a geometric effect, arising from the cross correlation between $(1+\delta_o)$ and $e(R_s)$. We perform the same analysis on numerical simulations with semi-analytical modeling (SAM) of galaxy formation. The e dependence of the galaxy properties shows similar behavior to that in the SDSS, although the color-density correlation is significantly stronger in the SAM. The 'optimal adaptive smoothing scale' in the SAM is also closely related to the distance to the 3rd-nearest-neighbor of a galaxy, and its characteristic value is consistent with, albeit slightly smaller than for SDSS.

Key words: galaxies: evolution - galaxies: formation - galaxies: stellar content

1 INTRODUCTION

While the standard picture of the hierarchical build-up of large-scale structure in the universe has been supported by ever increasing observational evidence, it is still an ongoing task to understand thoroughly the detailed baryonic physics associated with galaxy formation, such as gas accretion, star formation and feedback. Direct observation of these gaseous processes is challenging. On the other hand, given the large galaxy samples currently available to us, such as SDSS DR7 (Abazajian et al. 2009), statistical analysis of galaxy properties has proved to be invaluable to probe the underlying physics affecting galaxy formation and evolution.

The morphology-density correlation for galaxies, uncovered already in the 1930s (Hubble 1936), shows a clear segregation, with early-type galaxies preferentially existing in high density regions (Oemler 1974; Dressler 1978; Postman & Geller 1974; Blanton et al. 2005b; Kauffmann et al. 2004; Weinmann et al. 2006; Blanton & Berlind 2007; Park et al. 2007). Further investigation has indicated that

it is the star-formation related properties, such as color and emission-line flux, that are more directly correlated with environmental density (Kauffmann et al. 2004; Blanton et al. 2005b; Christlein & Zabludoff 2005). At fixed color, the residual dependence of morphology on the environmental density is rather weak (Park et al. 2007; Ball et al. 2008; Bamford et al. 2008). It is also emphasized by, e.g., Kauffmann et al. (2004), Blanton & Berlind (2007) and Park et al. (2007), that the environment dependence is in fact quite local. While galaxies with abundant close neighbors have clearly different properties from those of isolated galaxies, on scales larger than $\sim 1h^{-1}$ Mpc, environmental effects probably have little influence on galaxy properties (Blanton & Berlind 2007).

Theoretically, it has long been known from extensions of Press-Schecter theory that massive halos preferentially reside in dense environments (Bond et al. 1991; Mo & White 1996). Galaxies therein have properties that are different from those in small halos. On the other hand, the excursion set theory with sharp-k filter and with dynamics described by the spherical collapse model predicts that the formation history of halos of fixed mass should depend only on smaller-

* E-mail: yanheling1984@gmail.com

scale structure not on their large-scale environment (e.g., White 1996). Incorporating the ellipsoidal collapse model into excursion set theory gives halo mass functions and bias in better agreement with numerical simulations (Bond & Myers 1996; Sheth & Tormen 2001). In its simple version, however, the theory takes into account the ellipsoidal collapse by considering the average tidal field, and thus also predicts no correlations between the formation history of halos and their specific large-scale environment (Sheth & Tormen 2001).

Recent numerical simulations show that halo properties can be strongly correlated with their environment. Halo assembly bias reveals that old halos tend to cluster more strongly than their younger counterparts, and this bias is particularly significant for low mass halos (Gao et al. 2005; Harker et al. 2006; Wechsler et al. 2006; Gao & White 2007; Croton et al. 2007; Jing et al. 2007). Using filters other than the sharp-k filter in the excursion set theory leads to non-Markovian random walks, which in turn generate correlations between halo formation history and large-scale environment (e.g., Ma et al. 2010). Desjacques (2008) shows that under the spherical collapse model, the correlations arising purely from this non-Markovianity are expected to be stronger for more massive halos, in disagreement with the trend seen in simulations. Taking into account ellipsoidal collapse and the effects of large-scale environment on halo formation statistically (Sandvik et al. 2007) and dynamically (Desjacques 2008), the age dependent assembly bias can naturally arise and be more apparent for less massive halos. It is also noted by Desjacques (2008) that environmental density plays the determining role in the virialization redshift of halos, and that the morphology of large-scale structure contributes mostly to its scatter. However, given a fixed halo mass, the analytical model of Desjacques (2008) predicts that the median formation redshift of halos decreases with increasing environmental density, defined as the linear density fluctuation smoothed over $10h^{-1}$ Mpc. This is inconsistent with the results from simulations. Hahn et al. (2009) emphasize that for galactic-scale halos of fixed mass, an early formation epoch is closely related to a reduced mass-growth rate at late times that is mainly due to the tidal effects of neighboring massive halos. As galactic halos are enhanced in filaments near massive halos, the dependence of their formation epoch on environmental density is expected (see also, e.g., Diemand et al. 2007; Wang et al. 2007). For cluster-scaled halos, however, Dalal et al. (2008) show that tidal effects from large-scale structure cannot play an important role in the environment dependence of formation history.

Gas physics allows more complicated interactions between galaxies and their environment. Galaxies are more subject to ram pressure (e.g., Frenk et al. 1999) and shock heating (e.g., Mori & Burkert 2000) in denser regions. Both the cooling efficiency and the gas compression rate are directly related to environmental density. It has been observed in hydrodynamical simulations that most cold flows are highly anisotropic and follow dark matter filaments (e.g., Keres et al. 2005; Dekel & Birnboim 2006).

In this paper, we use SDSS DR7 data to examine the dependence of galaxy properties on their large-scale environment. We focus on the influence of the morphology of environment over and above the well-known dependence on

environment density. This analysis may provide important constraints on the theories and hypotheses discussed above. It can also help clarify if large-scale environment should be included in the halo occupation distribution model (e.g., Blanton & Berlind 2007; Tinker et al. 2008). The rest of the paper is organized as follows. In Section 2, we describe our measurements of large-scale tidal field with SDSS DR7. In Section 3, we present our results. Comparisons with results from simulations with semi-analytical modeling of galaxy formation are shown in Section 4. Section 5 contains discussions and our conclusions.

2   LARGE-SCALE TIDAL FIELD IN SDSS

2.1   SDSS and NYU-VAGC

The base data set adopted in this paper is SDSS DR7 (York et al. 2000; Abazajian et al. 2009). SDSS used a dedicated wide-field 2.5 m telescope (Gunn et al. 2006) located at Apache Point Observatory to obtain images in the u, g, r, i, z bands over an area of $\sim 10,000$ deg^2 and spectra of ~ 1.6 million selected objects among which galaxies amount to ~ 1 million. The photometric data was calibrated through ubercalibration (Padmanabhan et al. 2008), which used the overlap between adjacent imaging runs to tie together the photometry of all imaging observations. Fibers arranged on plates $1°.49$ in radius were assigned with an efficient tiling algorithm to spectroscopic targets selected with certain photometric criteria. Due to the fiber collision effect, only one spectroscopic measurement can be done for a group of targets with separations less than 55 arsec. Overlaps of tiles can help to reduce the number of missed targets. The overall incompleteness for galaxies is $\sim 6\%$. Our test shows that this incompleteness together with $< 2\%$ incompleteness caused by mismeasurement of redshift in spectra and bright star blocking is negligible for our measurements of the large-scale tidal field.

Our analysis is based on the large-scale structure sample VAGC dr72 of New York University Value Added Catalogue (NYU-VAGC;Blanton et al. (2005a)). It is constructed from SDSS, FIRST, 2MASS, 2dFGRS and PSCz. The SDSS part is updated for DR7. There are ~ 2.5 million galaxies in VAGC dr72. From VAGC dr72, we build up three volume-limited samples in which galaxies have absolute r-band magnitude brighter than $-18 + 5\log_{10}(h)$, $-19 + 5\log_{10}(h)$ and $-20 + 5\log_{10}(h)$ respectively, (M_r18, M_r19 and M_r20 hereafter). We consider all spectroscopic galaxies with listed apparent magnitude brighter than r = 18. All magnitudes mentioned in this paper are Petrosian magnitudes, and are K-corrected to redshift $z = 0$. For M_r18, M_r19 and M_r20, the respective number of galaxies is 26760, 53992 and 106033. We mainly focus on the M_r20 sample because its volume is large enough for accurate measurements of the large-scale structure geometry and it does not suffer galaxy bias severely since M_* in the luminosity function is a little brighter than -20.

The VAGC provides us information on the size and the stellar mass for each galaxy, so that we can directly draw four parameters, concentration $C = R_{90}/R_{50}$, $(g - r)$ color, stellar mass M_*, and the surface stellar mass density $\mu_* = M_*/(2\pi R_{50}^2)$, where R_{50} and R_{90} are defined as the radii
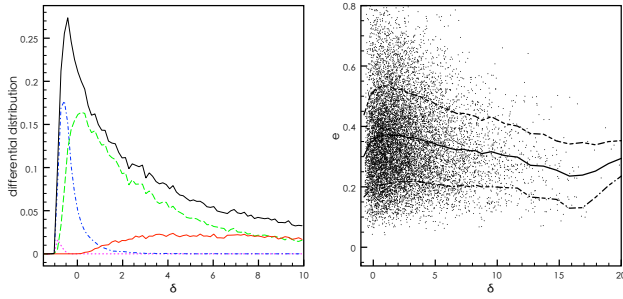
Figure 1. Left panel: The environmental density distributions for galaxies in eigenvalue-sign-judged halos (red solid line), filaments (green dashed line), sheets (blue dot-dashed line) and voids (magenta dotted line). The upper solid line shows the environmental density distribution for the whole sample. The smoothing scale for the environment of a galaxy is chosen to be the distance to its $3rd$ nearest neighbor. Right panel: Scatter plot of the environmental density δ and ellipticity e. The solid line is the average e at different δ and the dashed lines show $\pm 1\sigma$ e range around the average e.
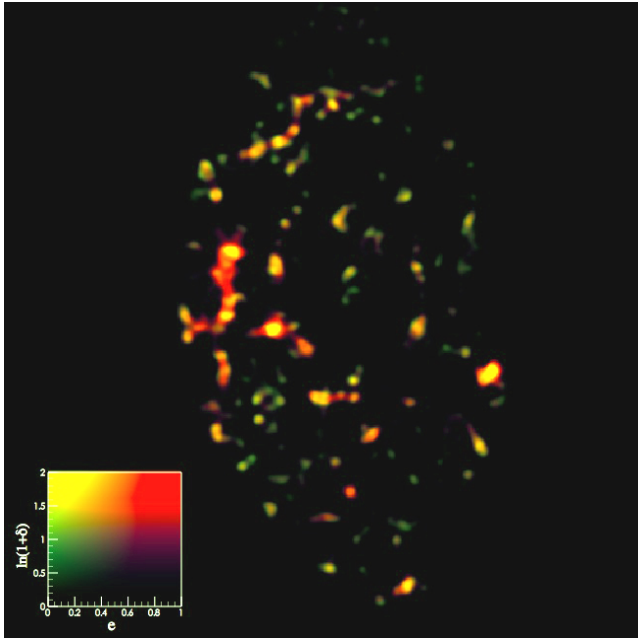

Figure 2. Contours of environmental $[e, \ln(1 + \delta)]$ for a slice of SDSS DR7. The environmental density and ellipticity are encoded with two-dimensional color scheme shown in the insertion. The smoothing scale is $3h^{-1}$ Mpc.

containing 50% and 90% of the Petrosian flux, respectively. In VAGC, calculations for the stellar mass M_* are based on five-band photometric data and redshift. Li & White (2009) compare this stellar mass measurement with spectroscopically based stellar mass measurements by Kauffmann et al. (2003), and show that the two results agree very well. We also add the amplitude of the 4000 $\mathring{A}$ break $D_n(4000)$ into our analysis as a clear indicator of stellar population age, from the MPA/JHU SDSS data (http://www.mpa-garching.mpg.de/SDSS/). There are 105034 galaxies in $M_r 20$ that have counterparts in MPA/JHU data set.

2.2 Tidal environment measurements

From a theoretical point of view, the tidal environment of a galaxy can be characterized by the second derivatives of the gravitational potential, $\partial_i \partial_j \phi$. The potential cannot, however, be measured directly, and needs to be calculated through the distribution of galaxies in redshift space. Such a measurement can be affected by, e.g., galaxy bias, redshift-space distortion and survey geometry. Here we describe our procedures to calculate the potential field, leaving detailed discussion to Section 4.

For calculations of the potential field, we put the volume-limited sample into a large cubic box with side $500h^{-1}$ Mpc. Galaxies are assigned onto a 512^3 uniform grid with CIC interpolation to give the number density of galaxies in each cell. We remove galaxies from those cells that happen to cross the survey boundary, and then assign the average number density of galaxies to all the empty cells. Filling the regions outside the survey volume with the average number density allows large voids with size comparable to the survey volume to be identified properly. This galaxy number density field is then smoothed with a Gaussian filter with a smoothing scale R_s, and the potential field, and further the tidal tensor field $\partial_i \partial_j \phi$ at each grid point are calculated from the smoothed density fluctuation field. The tidal environment of each galaxy is obtained by linearly interpolating this discrete tidal tensor field from the mesh to its position.

Without considering the specific orientation of the tidal tensor, its properties are fully characterized by its three eigenvalues $\lambda_1 \geqslant \lambda_2 \geqslant \lambda_3$. One way to classify the tidal environment of a galaxy uses the signs of λ_i $(i = 1, 2, 3)$ (e.g., Hahn et al. 2007; Zhang et al. 2009). Specifically, one can define a point as (i) "cluster", if all three eigenvalues are positive; (ii) "filament", if one eigenvalue is negative; (ii) "sheet", if two eigenvalues are negative; and (iv) "void", if all the three eigenvalues are negative. These definitions can show clearly the filament-node nature of large-scale structure at least in a two-dimensional cut. However, this classification is highly degenerate with a classification by density. As shown in the left panel of Figure 1, the overdensity distributions of points in these different categories are very different, and thus the dependence of galaxy properties on such "tidal environments" may mainly reflect a density dependence. To address the dependence of galaxy properties on tidal properties other than overdensity, we here describe the tidal environment of galaxies with parameters describing ellipticity e and prolateness p. Specifically, we define e and p as follows

$$e = \frac{\lambda_1 - \lambda_3}{3 + \delta}, \qquad p = \frac{\lambda_1 + \lambda_3 - 2\lambda_2}{3 + \delta},$$

where $\delta = \lambda_1 + \lambda_2 + \lambda_3$. We find that these definitions, with the number 3 added to the denominators, can minimize the correlations between e (p) and δ, as seen in the right panel of Figure 1. Figure 2 shows a 2-dimensional color rendering of $[e, \ln(1 + \delta)]$ in a 2-dimension cut through the $M_r 20$ sample. One can see that the cluster-filament-cluster structure is very well represented. High density and high ellipticity bridges link high density and low ellipticity clusters. In the following analysis, we mainly focus on the e-dependence of galaxy properties, since the δ-dependence has been well explored in previous work.
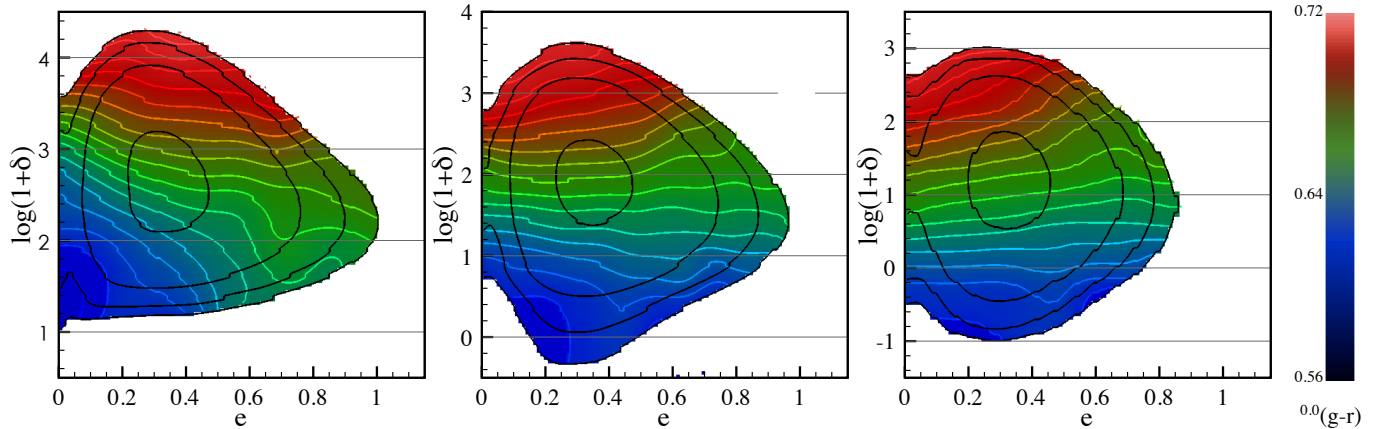
Figure 3. Galaxy color contours in the ellipticity-density plane for the SDSS DR7. The fixed smoothing scales are $1h^{-1}$ Mpc (left panel), $2h^{-1}$ Mpc (middle panel) and $3h^{-1}$ Mpc (right panel), respectively. The interval of the color contours is taken to be 0.05σ. The black rings are the uncertainty contours of galaxy color with values 0.05σ, 0.1σ, 0.15σ and 0.2σ from inside out, where $\sigma = 0.135$ is the standard deviation in galaxy color for the whole $M_r 20$ sample. The horizontal black lines are plotted so that the behavior of correlation/anticorrelation with ellipticity can be seen.
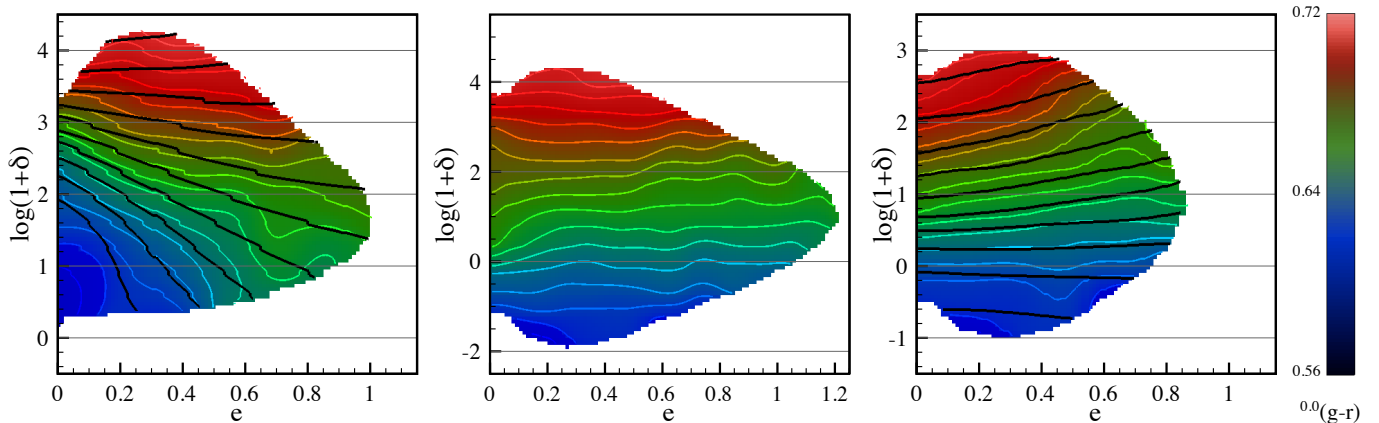

Figure 4. Galaxy color contours similar to Figure 3. The smoothing scales are $1h^{-1}$ Mpc (left panel), the 'adaptive smoothing scale' (middle panel) and $3h^{-1}$ Mpc (right panel), respectively. Here the 'adaptive smoothing scale' scale applied to smooth the environment of a galaxy is defined as the distance to its $3rd$ nearest neighbor. The black contours shown in the left and right panels are the contours of $\ln(1 + \delta_o)$ with δ_o the environmental density measured by this same optimal adaptive smoothing.

3 THE TIDAL DEPENDENCE OF GALAXY PROPERTIES

3.1 Tidal dependence of galaxy color

As can be seen from Figure 2, giant filaments link clusters together. These filaments have similar densities to the outskirts of clusters. By introducing the additional parameter e, however, these two regions can be separated clearly.

The main purpose of our study is to investigate if galaxy properties depend on the morphology of their large-scale environment in addition to the known density dependence. To do that, we consider galaxy properties in the $[e, \ln(1+\delta)]$ plane, and analyze the correlations of these properties with e and $\ln(1+\delta)$. Specifically, we divide the $[e, \ln(1+\delta)]$ plane into 128^2 cells, where $e \in [0, 1.2]$ and the typical range of $\ln(1+\delta)$ is $(-1, 4)$ with its precise range varying somewhat from one smoothing scale to another. We then extend the plane to a periodic 256^2 grid by reflecting the original cells

with respect to $e = 0$ and a line of the lowest value of $\ln(1+\delta)$. At each cell, we calculate the total number of galaxies $N[e, \ln(1+\delta)]$ and the sum of the considered galaxy property $C[e, \ln(1+\delta)]$. Smoothing is then applied to both C and N with a Gaussian smoothing function G_5, where subscript 5 denotes that the smoothing scale is 5 cells, and the average $\langle C \rangle_s$ is obtained at each grid point by $\langle C \rangle_s = C_s/N_s$, where the subscript s represents the smoothed quantities.

To quantify the statistical significance of the e-dependence of galaxy properties, we need to estimate the statistical errors for the smoothed quantities properly. Our sample contains ~ 0.1 million galaxies. When they are distributed onto 128^2 cells in the $[e, \ln(1 + \delta)]$ plane, we expect that Poisson fluctuations due to the limited number of galaxies associated with each cell will dominate the statistical errors. We thus estimate the error in each cell as $\sigma\sqrt{N_2}/N_1$, where σ is the standard deviation of the considered galaxy property over the whole sample, and N_1 and N_2

Table 1. Average value and standard deviation of different galaxy properties for $M_r 20$

Property	(g-r)	$-M_r$	$D_n 4000$	μ_*	R90/R50	M_*
mean	0.663	20.63	1.676	9.076	2.706	10.30
σ	0.135	0.481	0.259	0.376	0.433	0.256

are the smoothed cell count with the smoothing functions G_5 and G_5^2, respectively. In Table 1, we list the values of σ for different galaxy properties for $M_r 20$.

Figure 3 shows the results for the color $(g - r)$, where $\sigma = 0.135$ as derived from the sample $M_r 20$ and shown in Table 1. The three different panels correspond to three different smoothing scales to represent the large-scale environment, $R_s = 1h^{-1}$ Mpc, $2h^{-1}$ Mpc and $3h^{-1}$ Mpc from left to right. The $(g - r)$ values are shown in color in each panel with the scale shown to the right of Figure 3. For the superposed white contour lines, the interval between the adjacent lines is 0.05σ. The inside-out black lines show the error contours of 0.05σ, 0.1σ, 0.2σ and 0.3σ, respectively.

The dependence of $(g-r)$ on the density δ is clearly seen in Figure 3. The slope of the $(g-r)$ contours reflects whether the ellipticity e also affects the galaxy color in addition to δ. We can see a weak correlation between $(g-r)$ and e, and this correlation is scale-dependent. For $R_s = 1h^{-1}$ Mpc, an anti-correlation is seen. This reverses with increasing R_s, and is positive for $R_s = 3h^{-1}$ Mpc and larger. For $R_s = 2h^{-1}$ Mpc, the correlation is nearly null.

3.2 Scale-dependence of environmental effects

From Figure 3, we see that galaxy colors depend strongly on environmental density δ and weakly on environmental ellipticity e. This behavior are scale-dependent. The question arises then what smoothing scale one should adopt in order to reveal the most fundamental dependence of galaxy properties on their environment.

Previous studies have shown that galaxy properties are influenced by their environmental densities mainly locally (Kauffmann et al. 2004; Blanton & Berlind 2007; Park et al. 2007). On the other hand, if we simply smooth the environments on a scale larger than expected for any physical impact, we may still see an apparent environment-density dependence which arises merely due to the correlation between the environmental density on the considered smoothing scale and that on the scale where environmental effects are the strongest. This can also apply to the apparent e-dependence of galaxy properties shown in Figure 3.

The scale-dependent switch from anti-correlation to positive-correlation with e for galaxy colors seen in Figure 3 indicates to us that the best smoothing scale should be around the transition scale where no e-correlations are observed. Furthermore, this transition scale should correspond to the scale where the density dependence of galaxy properties is the strongest. In Appendix A, we discuss further this scale-dependence of the environmental-density influence on galaxy properties. We find that the scale where the environmental-density dependence of galaxy properties is the strongest is somewhat different for high and low density regions with the values of $\sim 1.5h^{-1}$ Mpc and

$2.5h^{-1}$ Mpc, respectively. This difference suggests that an adaptive smoothing scale may be more appropriate. A natural choice is the characteristic distance between the considered galaxy and its neighbors. Our analysis show that for $M_r 20$ sample, the distance to a galaxy's $3rd$-nearest-neighbor is an optimal adaptive smoothing scale, which has a distribution peaked at $2h^{-1}$ Mpc and is close to the peak scale where galaxy properties and environment density have the strongest correlation in both high and low density regions. For $M_r 19$ and $M_r 18$ samples, this optimal scale should correspond to the distance to a galaxy's $6th$-nearest- neighbor and $8th$-nearest-neighbor respectively, due to the fact that the galaxy density is higher.

In Figure 4, we show $(g - r)$ contours as in Figure 3. The right and left panels are for fixed smoothing scales of $1h^{-1}$ Mpc and $3h^{-1}$ Mpc, respectively. The middle panel shows results using the $3rd$-nearest-neighbor distance as an adaptive smoothing scale. In comparison with the middle panel of Figure 3, the null-dependence on e is more cleanly seen for the adaptive smoothing. To investigate if the dependence on e seen in the left and right panels of Figure 4 (the same as those of Figure 3) is physical or due to the correlations between (e, δ) at the considered scale and δ at the 'optimal adaptive smoothing scale', we calculate the latter correlations. Specifically, we define (e, δ) at the considered smoothing scale and at the optimal adaptive smoothing scale as (e_a, δ_a) and (e_o, δ_o), respectively. We compute the δ_o-contours in the (e_a, δ_a) plane, which are shown as black lines in the left and right panels of Figure 4. It is seen that the δ_o-contours align with the $(g - r)$-contours (white lines) very well. This demonstrates that the observed e-dependence is mainly attributable to the correlation between (e_a, δ_a) and δ_o. Some deviation between the $(g - r)$-contours and the δ_o-contours are seen in high density regions. These are, however, insignificant compared to the statistical errors. Together with the null-correlation with e for the optimal adaptive smoothing, we conclude that no significant physical dependence of galaxy colors on e is detected by our analysis.

3.3 Other galaxy properties

We have studied the dependence of galaxy color on (e, δ) carefully. Here we examine the tidal dependence of other galaxy properties.

Galaxy properties can be divided into three classes: (1) star-formation-related properties such as galaxy color and $D_n(4000)$; (2) morphology-related properties such as concentration; and (3) extensive quantities such as the total stellar mass M_* and galaxy size. Previous studies have shown that star-formation-related properties depend directly on the environmental density (Kauffmann et al. 2004; Blanton et al. 2005b; Christlein & Zabludoff 2005), but morphology-related ones are not independently correlated with environmental density (Park et al. 2007; Ball et al. 2008; Bamford et al. 2008).

Here we analyze the (e, δ)-dependence of different galaxy properties. Figure 5 presents the environmental dependence of $(M_*, D_n 4000)$. The left panel shows a scatter plot of $(M_*, D_n 4000)$. The red lines are contours of constrained mean value of $\ln(1 + \delta_o)$. From the scatter plot, we see that $D_n 4000$, which reflects stellar population ages
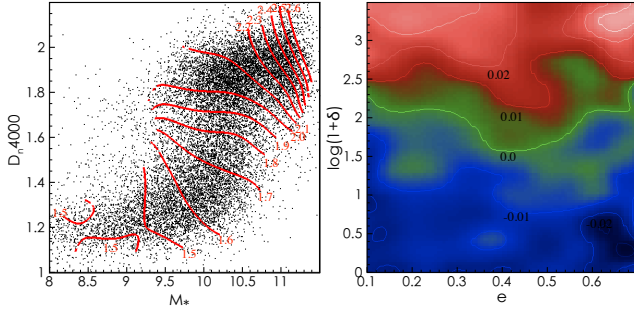
Figure 5. Left panel: The scatter plot of $(M_*, \mathrm{D}_n(4000))$. The $\ln(1 + \delta_o)$ contours are shown in red. Right panel: The contours of $\mathrm{D}_n(4000)$-$\langle \mathrm{D}_n(4000) \rangle$, where $\langle \mathrm{D}_n(4000) \rangle$ is the average value of $\mathrm{D}_n(4000)$ given stellar mass.

Figure 6. Left panel: The scatter plot of $(\mathrm{D}_n(4000), C)$. The $\ln(1 + \delta_o)$ contours are shown in red. Right panel: Contours of $C - \langle C \rangle$, where $\langle C \rangle$ is the average value of C given $\mathrm{D}_n(4000)$.

and therefore star formation histories, correlates with total stellar mass M_*. The directions of the red contours indicate that both depend on environmental density as measured by our optimal adaptive smoothing. In the right panel of Figure 5, we show the (e, δ) dependence for D_n4000 given the stellar mass M_*. Specifically, the contours of the deviation $\mathrm{D}_n4000 - \langle \mathrm{D}_n4000 \rangle$ are shown, where $\langle \mathrm{D}_n4000 \rangle$ is the average value of D_n4000 in stellar mass bins. The environmental-density dependence of the contours are clearly seen, which, in agreement with the trend seen in the left panel, demonstrates the extra density dependence of D_n4000 in addition its dependence of M_*. On the other hand, no dependence on the shape parameter e is detected.

In Figure 6, we show a similar analysis for the concentration parameter $C = R_{90}/R_{50}$. The scatter plot of (D_n4000, C) is shown in the left panel with the $\ln(1 + \delta_o)$ contours superposed on it. Two clumps are seen in the scatter plot with one at low value of D_n4000 and small value of C, and the other at high D_n4000 and large C. The lower-left clump corresponds to galaxies with recent star formation, and the upper-right clump is associated with galaxies with quenched star formation. The $\ln(1 + \delta_o)$ contour lines are nearly vertical, showing no detectabe independent correlation between C and the environmental density. In the right panel of Figure 6, we show the $C - \langle C \rangle$ contours in the $[e_o, \ln(1 + \delta_o)]$ plane, where $\langle C \rangle$ is the average value of C given D_n4000. The chaotic pattern seen here reflects the lack of any environmental dependence of the concentration C other than its δ_o dependence through the correlations with D_n4000.

We also analyze the environmental dependence of galaxy size defined as R_{50}*d in unit of h^{-1}kpc, where d denotes the distance to a galaxy. The results are shown in Figure 7, again using our optimal adaptive smoothing. It is seen that in high density regions, galaxy size has no detectable correlation with either environmental density or ellipticity. In low density regions, on the other hand, there is a notable correlation between galaxy size and e_o in addition to its correlation with δ_o. We will show in section 4.3 that in low density regions, the survey boundary effects can bias the δ_o and e_o measurements to lower values. This can induce an artificial correlation with e_o, which is considerable for small-volume samples such as M_r18. For M_r20, however, the survey volume is large and the boundary effects are insignificant. Thus the correlations seen in the lower left
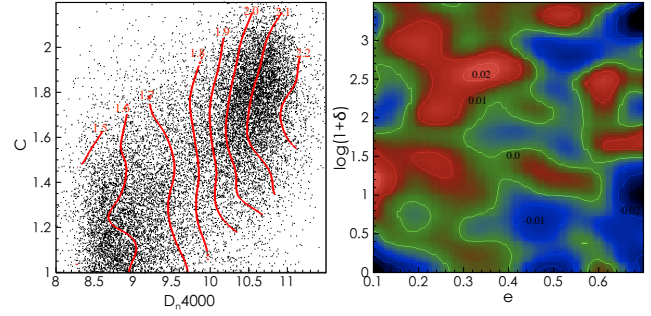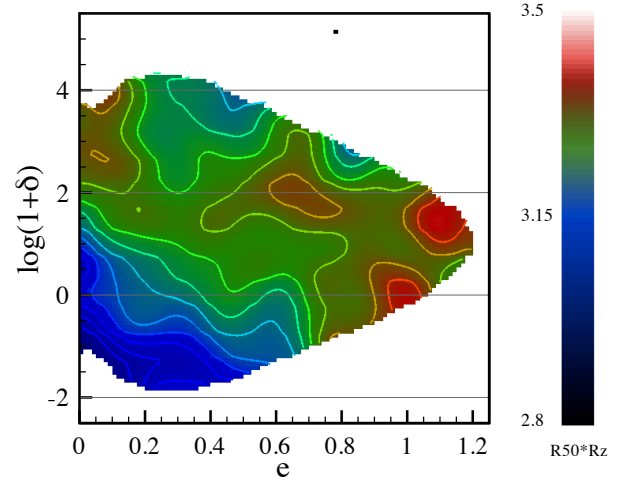

Figure 7. Contours of galaxy size defined as $R_{50} * R_z$ in unit of for SDSS. The boundary is the 0.2σ uncertainty contour, where σ is the standard deviation of galaxy size for the whole sample. The optimal adaptive smoothing is applied.

region of Figure 7 may indicate that both the density and the ellipticity of the environment, can affect the galaxy size. Galaxies are systematically smaller in lower (δ_o, e_o) regions. Due to the still limited statistics of SDSS, the environmental e_o dependence of galaxy size needs to be investigated further with future large surveys that can provide much improved statistics.

Our analysis so far has measured ellipticity and density on the same scale. The optimal adaptive smoothing is chosen to be the distance from a galaxy to its 3rd-nearest neighbor. This scale has a distribution peaked between $1.5\mathrm{h}^{-1}\mathrm{Mpc}$ and $2.5\mathrm{h}^{-1}\mathrm{Mpc}$, depending on environmental density. In order to show the influence of larger scales, especially the influence of the large filaments linking cluster as seen in Figure 2, we also analyze the environmental dependence of galaxies properties on ellipticity and density measured on two different scales. We fixs the smoothing for density to the optimal adaptive smoothing and we change the smoothing scale for ellipticity. For no smoothing scale larger than the $2\mathrm{h}^{-1}\mathrm{Mpc}$ do we see a correlation of galaxy properties with environment ellipticity. We thus conclude that large scale structure beyond galaxy groups has no additional influence on individual galaxies.

We have so far focused our analysis on the ellipticity e of large-scale environment. However, we have also looked for the dependence of galaxy properties on the environmental prolateness p. We find that smoothing according to the distance to the $3rd$-nearest-neighbor of a galaxy, all of the considered galaxy properties are independent of p.

4 COMPARISON WITH A SEMI-ANALYTIC MODEL

In semi-analytic models of galaxy formation (SAM), our best understanding on dark matter halo formation is combined with the complex baryonic physics associated with galaxy formation as represented by physically/observationally motivated prescriptions involving a set of parameters. While earlier SAMs were based on using the extended Press-Schechter theory to construct dark matter halo merger trees, modern SAMs take full advantage of high resolution N-body simulations to follow the formation and evolution of dark matter halos. Galaxies are then formed within these halos by modeling physical processes such as cooling, condensation, star formation, supernova and AGN feedback. Here we analyze the SAM galaxy catalog from De Lucia & Blaizot (2007), for which the dark matter distribution was taken from the Millennium Simulation (Springel et al. 2005). We compare the results with those from the SDSS. To test observational effects, we also construct mock SDSS DR7 catalogs from the SAM data (Li et al. 2007) . Specifically, we address the following issues

(i) a comparison of the environmental-density dependence of galaxy properties in the SAM and the SDSS;

(ii) a comparison of the behavior of the tidal dependence of galaxy properties;

(iii) the influence of various observational effects, such as redshift-space distortion and survey geometry on the results of our tidal analysis.

4.1 Scale dependence of the color-density relation in the SAM

To analyze the scale dependence of the color-density relation, we calculate the correlation coefficient between galaxy color $(g−r)$ and environmental density δ at different smoothing scales. The correlation coefficient is defined as

$$r = \frac{\langle \Delta(g-r)\Delta\delta_o \rangle}{\sqrt{\langle [\Delta(g-r)]^2 \rangle}\sqrt{\langle (\Delta\delta_o)^2 \rangle}},$$

where $\Delta(g-r) = (g-r) - \langle (g-r) \rangle$ and $\Delta\delta_o = \delta_o - \langle \delta_o \rangle$. The results are shown in Figure 8. We divide galaxies into two groups of high (solid lines) and low densities (dashed lines) as described in Appendix A (the green lines in Figure A1). The red, blue and green lines are, respectively, for the SDSS, the full volume of the SAM, and for the mock SDSS.

First, we see similar trends for the scale dependence of the color-density correlation in the SAM and the SDSS data. The SAM 'optimal smoothing scale' for the strongest correlation is also consistent with that of SDSS, which is $\sim 1h^{-1}$ Mpc for high density regions and $\sim 2h^{-1}$ Mpc for low density regions. On the other hand, the amplitude of the correlation coefficient is significantly larger for the SAM
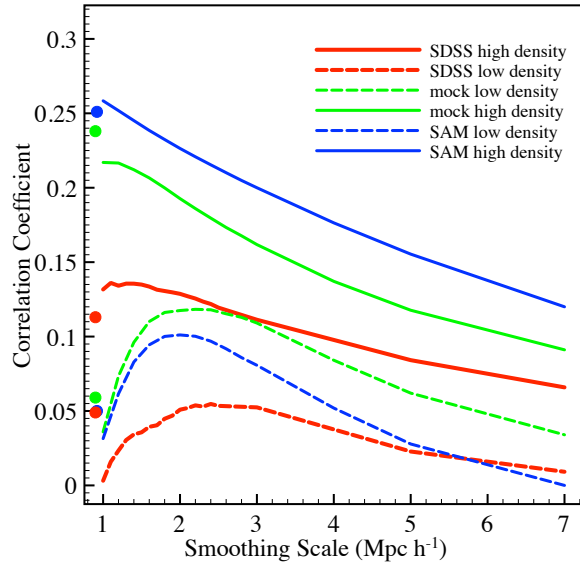

Figure 8. The color-density correlation coefficient as a function of smoothing scale. The red, blue and green lines give results for SDSS, SAM, and mock catalog, respectively. The solid and dashed lines are the results for galaxies in high and low density regions, respectively (see Appendix A). The filled circles of different color represent the results for optimal adaptive smoothing of the corresponding samples.

than for the SDSS. The SAM predicts an environment-density dependence of galaxy colors stronger than is observed, in accordance with other studies (e.g., Springel et al. 2005; Coil et al. 2008; Font et al. 2008; Cowan& Ivezić 2008; Guo et al. 2011). We note that while the tidal interactions of dark matter halos are naturally accounted for in the SAM, tidal disruption of galaxies is not. For massive clusters, however, it is expected that their strong tidal forces may destroy galaxies (e.g., Henriques et al. 2008). As those satellite galaxies are mostly red, such disruptions can decrease the level of clustering of red galaxies, and therefore reduce the discrepancies in color-density relation between the SAM and the observations in high density regions. Further, this can also alleviate the overly-fast-growth problem for central galaxies in the SAM (Wang & Jing 2010). It has also been argued that hot gas in satellite galaxies may not be immediately stripped away by ram pressure when they merge into a larger system as often assumed in SAMs. Therefore a reservoir of gas can be replenished to maintain the star formation for a relatively long period of time (e.g., Font et al. 2008; Coil et al. 2008; Weinmann et al. 2006; Guo et al. 2011). In low density regions, the SAM also predicts stronger color-density correlations than seen in the SDSS, which reflects the smaller color spread in the SAM compared to the SDSS.

The green lines in Figure 8 are the results from the SDSS DR7 mock catalogue constructed from SAM data. The differences between the green and blue lines reflect observational effects which will be discussed in §4.3.
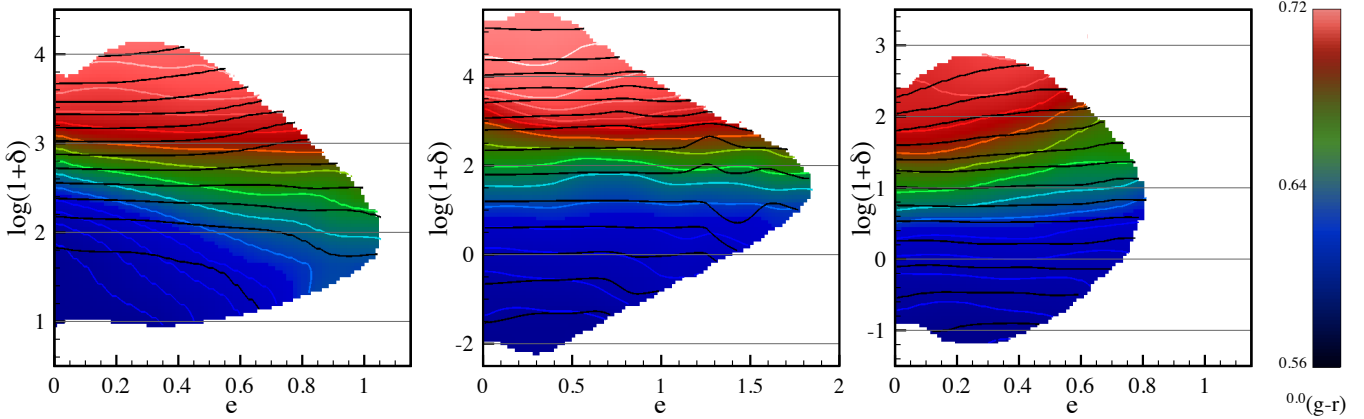
Figure 9. Galaxy color contours similar to Figure 4, but for the SAM. Here the black contours are the color contours for mock data. The smoothing scales are $1h^{-1}$ Mpc (left panel), distance to the $3rd$-nearest-neighbor (middle panel) and $3h^{-1}$ Mpc (right panel), respectively. The outer boundary is the uncertainty contour of galaxy color with the value of 0.1σ, where $\sigma = 0.157$ is the standard deviation of the galaxy color distribution for the whole SAM sample.

4.2 Tidal dependence of galaxy properties in SAM

To study the tidal dependence of galaxy properties, we perform the same analysis for the SAM data as shown in §3.2 for the SDSS. The results are shown in Figure 9. The black lines here represent results from the mock catalogue, and will be discussed in §4.3. The three panels correspond to the smoothing with $R_s = 1h^{-1}$ Mpc, with the $3rd$-nearest-neighbor distance, and with the $R_s = 3h^{-1}$ Mpc. It is seen that the contour behaviors are qualitatively similar to those of Figure 4 for the SDSS. In the SAM, the distance to the $3rd$-nearest neighbor also corresponds to the 'peak scale' of the color-density dependence, at which, the tidal e-dependence of galaxy properties is nearly null. The density δ_o at the optimal adaptive smoothing scale plays the dominant role for the environmental effects. The weak negative/positive $(g-r)$-e correlations at smaller/larger smoothing scales again reflect correlations between (e, δ) at the smoothing scale and δ_o.

A notable difference between Figure 9 and Figure 4 is the density dependence of color, which is significantly stronger in Figure 9 than that shown in Figure 4. This is consistent with the result shown in Figure 8, which also show that the SAM predicts a considerable stronger color-density correlation than seen in observations.

4.3 Observational effects

To make a realistic comparison between the results for the SAM and the SDSS, different observational effects must be taken into account. We thus build mock catalogs from the SAM data following Li et al. (2007). We first test the influence of fiber collisions which reduce the number of redshift measurements for galaxies in close pairs by about 6%. Because our smoothing scale is nearly always larger than $55''$, fiber collisions do not affect our analysis significantly.

The most notable influences from obervations are the redshift distortion effect and the effect from the survey geometry. The redshift-space distortion affects mainly the high

density regions and plays a role of "mixing". In redshift space, galaxies in massive clusters present a Finger-of-God configuration along the line of sight. On the other hand, galaxies in filaments surrounding a massive cluster have a tendency to be flowing into the cluster, which squashes the filaments along the line of sight. In other words, galaxies in filaments and galaxies in massive clusters are somewhat mixed in redshift space. Thus the color scatter in a given density bin becomes larger in redshift space, resulting in a lower color-density correlation coefficient in high density regions, as shown by the green solid line in Figure 8. Furthermore, the redshift-space distortion makes the measured environmental density systematically lower than that measured in real space. The ellipticity calculated in the redshift space is systematically lower/higher for regions with high/low e in real space. That is, filaments become rounder and clusters tend to be more anisotropic in redshift space. Such effects cause color mixing in the $[e, \ln(1 + \delta)]$ plane, and thus lead to flatter color contours with respect to the ellipticity e and weaker correlations with δ (see the black contour lines in Figure 9).

In low density regions, measurements of environmental density and ellipticity are mainly affected by survey geometry. Both are biased to lower values. In the left panel of Figure 10, we show the value of e with respect to the distance to the survey boundary for SDSS sample M_r20. Different lines represent different environmental density ranges with longer dashes corresponding to higher densities. Physically, we do not expect any correlations between e value and the distance to the survey boundary. For high-density lines, they are indeed nearly flat. For low-density lines, however, the measured e is systematically lower for galaxies closer to the survey boundary. The effect is significant for galaxies that are within $20h^{-1}$ Mpc of the boundary. This is clearly an observational effect due to padding the regions outside the survey boundary with the average number density. Such a measurement bias on e can lead to artificial correlations between galaxy properties and environmental ellipticity. The significance of the effect depends on the the fraction of galaxies that are within $20h^{-1}$ Mpc of the boundary. Volume-limited

samples with smaller volume are affected more. In the right panel of Figure 10, we show the ratio of color in high e regions to the color in low e regions vs. minus the absolute magnitude of galaxies -M_r. Here high and low e are defined as above the 1σ level and below the -1σ level with respect to the average e (see the right panel of Figure 1). We present results for different SDSS volume-limited samples, M_r18, M_r19 and M_r20 from smaller to larger volume. For M_r18, we see the decrease of the color ratio with respect to -M_r of galaxies. That is, for relatively faint galaxies, the ones in low e regions tend to be bluer than those in high e regions. For bright galaxies, the ratio is close to 1. For M_r19 and M_r20, there is no detectable dependence of the color ratio on -M_r, and the ratio is always close to 1. To test if the M_r-dependence of the color ratio seen in M_r18 is physical or due to the boundary effect, we construct subsamples of galaxies with distances less than $110h^{-1}$ Mpc from M_r19 and M_r20, respectively. This cut corresponds roughly to the distance limit of M_r18. The results for the M_r19 and M_r20 subsamples are shown by unfilled green triangles and unfilled red squares, respectively. The apparent correlation with M_r of galaxies is then seen. This demonstrates that the correlation seen for M_r18 sample is largely due to the boundary effect. As shown in the left panel of Figure 10, in low density regions, the e value is biased to a lower value for galaxies closer to the survey boundary. Because galaxies in low density regions tend to be bluer than those in high density regions, this bias leads to an increase in the number of relatively blue galaxies in low e regions, and thus increases the color ratio between high e and low e regions. The increase of the color ratio is more significant for fainter galaxies because the observed ones reside in a smaller volume around the observer and thus suffer more from the boundary effect.

In Figure 11, we show color contours in the $[e_o, \ln(1 + \delta_o)]$ plane for M_r18. For M_r18, the optimal adaptive smoothing scale for a galaxy corresponds to the distance to its 8th nearest neighbor. Comparing to the middle panel of Figure 4, we see a notable correlation between color and ellipticity in low-density regions. This however, is largely due to the survey boundary effect that biases both the environmental density and ellipticity toward lower values in low density regions.

5 CONCLUSION AND DISCUSSION

In this paper we examine the tidal dependence of galaxy properties in the NYU-VAGC sample and compare it with the predictions of the SAM. To separate the environment-morphology dependence from the environmental-density dependence, we construct the density fluctuation δ, the ellipticity e and the prolateness p from the three eigenvalues of the tidal tensor of the potential field calculated from the spatial distribution of galaxies, where e and p are nearly independent of δ. It should be noted that this potential field can be biased with respect to the potential field from the underlying dark matter distribution. The well-known galaxy bias refers to the ratio of the density fluctuation amplitude of galaxy distribution and that of the dark matter distribution.

For M_r20, the volume-limited sample with absolute magnitude brighter than -20, our results show that while the environmental-density dependence of galaxy properties
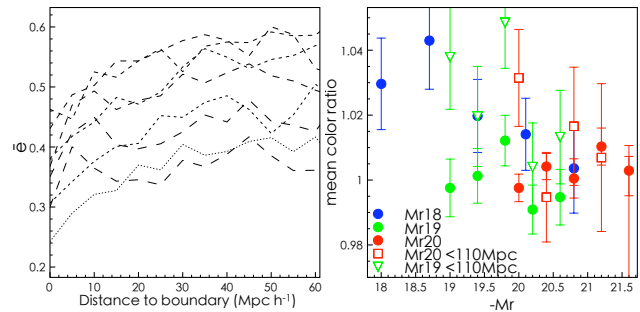

Figure 10. Left panel: The average environment ellipticity for galaxies as a function of their distance to the survey boundary. The optimal adaptive smoothing has been applied. Different lines represent the results for different bins of $log(1 + \delta_o)$ ranging from $\log(1 + \delta_o) = -2.0$ to $\ln(1 + \delta_o) = 4.0$. Longer-dashed lines represent the results for higher density bins. Right panel: The ratio of the mean $(g-r)$ in high ellipticity regions to that in low ellipticity regions for M_r 20 (red filled circle), M_r19 (green filled circle) and M_r18 samples (blue filled circle), respectively. The high and low ellipticity regions are defined as the regions above the $+1\sigma$ dashed line and below the -1σ dashed line shown in the right pane of Figure 1. The results for subsamples of M_r20 and of M_r19 cut at $110h^{-1}$ Mpc are shown by red open squares and green open triangles, respectively.
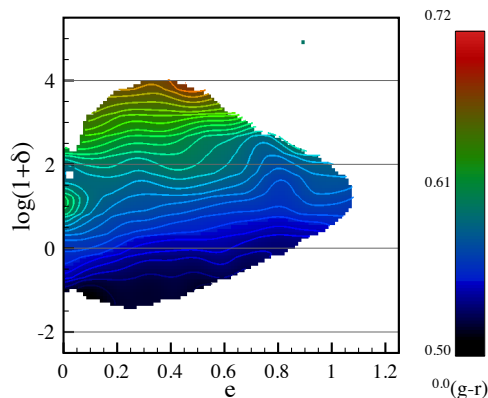

Figure 11. Galaxy color contours for SDSS M_r18. The environmental smoothing scale for a galaxy is taken to be the distance to its 8th-nearest neighbor. The boundary is the 0.3σ uncertainty contour, where $\sigma = 0.168$ is the standard deviation of galaxy color of the whole M_r18 sample.

is indisputable, the dependence on e and p is rather weak, except perhaps for galaxy size. It is further shown that such weak correlations depend on the smoothing scale considered for the environment. There exists a particular scale, $\sim 2h^{-1}$ Mpc, at which, the environmental-e (p) dependence nearly vanishes. This corresponds to the optimal adaptive smoothing scale where the environmental-density dependence of galaxy properties is the strongest. It varies from high density regions to low density regions, and corresponds well to the distance to each galaxy's $3rd$-nearest-neighbor for M_r20 sample. At smoothing scales larger/smaller than this 'optimal smoothing scale', the weak correlations between galaxy properties and e are negative/positive. We demonstrate, however, that these correlations result mainly

from correlations between (e, δ) at the considered smoothing scale and the environmental density δ_o at the optimal adaptive smoothing scale. In other words, we find no physical influence of environment morphology on galaxy properties. Furthermore, it is δ_o that plays the dominant role for the environmental effects, and the apparent density dependence on other smoothing scales is largely due to the correlations between δ and δ_o. This indicates that, galaxy properties in $M_r 20$ are affected mainly by their nearby environments. Our analysis shows that galaxy size is independent of environment in high-density regions. In low-density regions, some correlation with e_o in addition to the dependence on δ_o is detected. Galaxies in lower (δ_o, e_o) regions tend to be smaller. Such correlations need to be further explored with future observations.

With NYU-VAGC $M_r 19$, Blanton & Berlind (2007) analyze galaxies in groups, and find that galaxy properties depend mainly on the properties of their host groups, and are not affected independently by the environment on larger scales($> 1h^{-1}$ Mpc). As they only consider galaxies in groups, it is appropriate to compare their results with ours in high density regions. From Figure 8, we can see that the 'peak scale' in high density regions is $\sim 1h^{-1}$ Mpc, consistent with the typical group scale in their studies. Therefore our results are in agreement with theirs concerning the dominant importance of the nearby environment. This in turn validates the current halo occupation distribution model, which assumes that galaxy properties depend only on those of their parent halos with no additional influence from larger scale. Lee & Lee (2008) also examines the tidal dependence of galaxy properties. They found that there is a tendency for elliptical galaxies to be preferentially situated in low e regions with density in the range $0.5 \leqslant \delta \leqslant 1.06$. For $-0.3 \leqslant \delta \leqslant 0.1$, spiral galaxies are likely in regions with large e. We note that their considered scale for environmental effects is $\sim 400/64 \sim 6h^{-1}$ Mpc. Thus their results can loosely be compared with our analysis for $R_s = 3h^{-1}$ Mpc (but note the different δ range). With the correspondence between color and morphology of galaxies, the positive correlation of galaxy color with e seen in right panel of Figure 4 is qualitatively consistent with the trend found by Lee & Lee (2008) although their definition of e is different from ours. On the other hand, our analysis indicates that this e-dependence is largely due to the correlations between e and δ_o and therefore has little physical significance.

Comparing the SDSS results with those from our SAM, we see qualitative agreement between the two, although the SAM predicts a stronger dependence of galaxy properties on environmental density. Our results are also in accordance with the theoretical study of Desjacques (2008), which showed that environmental effects on dark matter halo formation mainly reflect environmental density, and are influenced little by e and p. Hahn et al. (2009) found that the anti-correlation between the formation epoch of galactic halos and their environment density is, in fact, mainly attributable to tidal suppression by neighboring massive halos. Because of the enhanced environment density near massive halos, this suppression shows up as an assembly bias, and provides a possible explanation for galaxy variation with environment density. On the other hand, Hahn et al. (2009) chose the smallest eigenvalue λ_3 of the tidal tensor as an indicator of the strength of tidal field, and they found a

stronger dependence of halo formation epoch on λ_3 than on environment density. Our results manifest a strong degeneracy between λ_3 and environment density. Just as for ellipticity, λ_3 can be geometrically more strongly correlated with environment density on the optimal smoothing scale than on a larger scale. Further work is needed to clarify whether the dependence of halo formation history on environment morphology can be attributed to this geometry effect, or whether baryon physics actually make difference between halos and galaxies.

By constructing mock catalogs from SAM data, we have examined the influence of observational effects on our analysis. Redshift-space distortion is significant in high density regions. It mixes galaxies in filaments and galaxies in clusters causing an increase of color scatter at given density, and therefore reduces the color-density correlation coefficient considerably. The survey boundary affects environment measurements mainly in low density regions, biasing both the environmental density and the ellipticity to lower values. The effect is notable for galaxies within $20h^{-1}$ Mpc of the survey boundary. While it is negligible for $M_r 20$, the effect is considerable for $M_r 18$ which occupies a relatively small volume and therefore has a large fraction of its galaxies close to the boundary. It induces an artificial correlation between galaxy properties and the environmental ellipticity for $M_r 18$.

In summary, our analysis of SDSS data shows that in addition to environment density, there is no significant further dependence of galaxy properties on the morphology of large scale structure. Geometrically, both ellipticity and density on one smoothing scale correlate strongly with each other, and with ellipticity/density on other smoothing scales. If the smoothing scale is not chosen properly, an appeared dependence of galaxy properties on both environment ellipticity and environment density arises which is merely due to geometry. We find that for the optimal adaptive smoothing scale, the dependence on density is maximized and the dependence on ellipticity and prolateness is null.

REFERENCES

Abazajian K., Adelman-Mccarthy J.K., Agueros, M., 2009, ApJS, 182, 543

Ball N.M., Loveday J., Brunner R.J., 2008, MNRAS, 383, 907

Bond J.R., Myers S.T., 1996, ApJS, 103, 1

Bamford S.P., Rojas, A.L., Nichol R.C., 2008, MNRAS, 391, 607

Blanton M.R., Schlegel D.J., Strauss M.A., 2005, ApJ, 128, 2562

Blanton M.R., Eisenstein D., Hogg D.W., 2005, ApJ, 629, 143

Blanton M.R., Berlind A.A., 2007, ApJ, 664, 791

Bond J.R., Efstathiou G., Kaiser N., 1991, ApJ, 379, 440

Christlein D., Zabludoff A., 2005, ApJ, 621, 201

Coil A., Newman J.A. & Croton D., 2008, ApJ, 672, 153

Cowan N.B., Ivezi C Ž., 2008, ApJ, 674, 13

Dalal N., White M., Bond J. R., Shirokov A., 2008, ApJ, 687,12

Dekel A. Birnboim Y., 2006, MNRAS, 368,2

De Lucia G., Blaizot J., 2007, MNRAS, 375, 2

Desjacques V., 2008, MNRAS, 388, 638

Diemand J., 2007, ApJ, 667, 859

Dressler, A., 1978, ApJ, 223,765

Croton D.J., Gao L., White S.D.M., 2007, MNRAS, 374, 1303

Gao L., Springel V., White S.D.M., MNRAS, 363, 66

Gao L., White S.D.M., 2007, MNRAS, 377, 5

Gunn J.E., Siegmund W.A., Mannery E.J., 2006, AJ, 131, 2332

Guo, Q., White, S.D.M., Boylan-Kolchin, M., & De Luica, G., 2011, MNRAS, 413, 101

Frenk C.S., White S.D.M., Bode P., ApJ, 525, 554

Font A.S., Bower R.G., McCarthy I.G., MNRAS, 389, 1619

Hahn O., Corollo M., Porciani C., 2007, MNRAS, 381,41

Hahn O., Porciani C., Dekel A., 2009, MNRAS, 398, 1742

Henriques B. M., Bertone, S., Thomas P.A., 2008, MNRAS, 383, 1649

Hubble E.P., 1936, The Realm of the Nebulae. New Haven, CT: Yale Univ. Press

Harker G., Cole S., Helly J., 2006, MNRAS, 367, 1039

Jing Y.P., Suto Y., Mo H.J., 2007, ApJ, 657, 665

Kauffmann G., Heckman T.M., White S.D.M.

Kauffmann G., White S.D.M., Heckman T. M., 2004, MNRAS, 353, 713

Keres D., Katz N., Weinberg D.H., 2005, MNRAS, 363, 2

Keselman J.A., Nusser A., 2007, MNRAS, 382, 1853

Kim H.S., Baugh C.M., Cole S., 2009, MNRAS, 400, 1527

Lacey C., Cole S., 1993, MNRAS, 262, 627

Lee J., Lee B., 2008, ApJ, 688, 78

Li C., Kauffmann G., Jing Y.P, 2006, MNRAS, 368, 21

Li C., Jing Y.P, Kauffmann G., 2007, MNRAS, 376, 984

Li C., White S.D.M., 2009, MNRAS, 398, 2177

Ma C. P., Maggiore M., Riotto A., Zhang J., 2010, MNRAS in press (arXiv:1007.4201)

Mo, H. J. & White, S.D.M., 1996, MNRAS, 282, 347

Mori M., Burkert A., 2000, ApJ, 538, 559

Park C., Choi Y.Y., Vogeley M.S., 2007, ApJ, 658, 898

Sandvik H.B., Möller

Sheth R.K., Mo H.J., Tormen G., 2001, MNRAS, 323

Somerville R.S., Lemson G., Sigad Y., 2001, MNRAS, 320, 289

Springel V., White S.D.M., Jenkins A., 2005, Nature, 435, 629

Oemler A., 1974, ApJ, 194, 1

Padmanabhan N., Schlegel, D.J., Finkbeiner D. P. et al., 2008, ApJ, 674, 1217

Postman M., Geller M.J., 1984, ApJ, 281, 53

Tinker J.L., Conroy C., Norberg P., 2008, ApJ, 686, 53

York D.G., Adelman J., Anderson J.E., 2000, AJ, 120, 1579

Wang H.Y., Mo H.J., Jing Y.P., 2007, MNRAS, 375, 633

Wang L., Jing Y.P., 2010, MNRAS, 402, 1796

Wechsler R.H., Zentner A.R., Bullock J.S.

White S. D. M., 1996, in Schaeffer R., Silk J., Spiro, M., Zinn-Justin J., eds, Les Houches Session LX, Cosmology and Large Sclae Structure. Elsevier, Amsterdam, p.77

Weinmann S.M., van den Bosch F.C., Yang X.H., Mo H.J., 2006, MNRAS, 366 2

Zhang Y.C., Yang X.H., Faltenbacher A., 2009, ApJ, 706, 747

This paper has been typeset from a TeX/ LaTeX file prepared by the author.

APPENDIX A: SCALE DEPENDENCE OF COLOR-DENSITY RELATION

Previous studies have shown that age-related properties, such as galaxy color, are correlated with environmental density and that this correlation is scale dependent (Kauffmann et al. 2004; Blanton & Berlind 2007; Park et al. 2007). Here we examine the scale dependence of the color-density relation quantitatively and in more detail.

For each galaxy, we calculate its environmental density at two different smoothing scales, denoted as δ_{R_1} and δ_{R_2}. We then analyze the dependence of galaxy color on $(\delta_{R_1}, \delta_{R_2})$. The results are shown in Figure A1, where $R_1 = 2h^{-1}$ Mpc is taken to be the reference scale. In each panel, the black dots show the values of $[\ln(1 + \delta_{R_1}), \ln(1 + \delta_{R_2})]$ for all the galaxies, and the red lines are $(g - r)$ contours. The green line denotes our dividing line for high and low density regions, which is the -45° line passing through the point of $(1.0, d_0)$, where d_0 is the corresponding value of $\ln(1 + \delta_{R_2})$ given $\ln(1 + \delta_{2Mpch^{-1}}) = 1.0$. It is seen that for $R_2 \geqslant 5h^{-1}$ Mpc, the color-density dependence, $(g - r) - (\delta_{2Mpch^{-1}}, \delta_{R_2})$, is mainly on $\delta_{2Mpch^{-1}}$, and the additional dependence on δ_{R_2} is very weak. For $R_2 = 3h^{-1}$ Mpc, a certain level of δ_{R_2}-dependence is seen in low density regions. For $R_2 = 1h^{-1}$ Mpc, on the other hand, the δ_{R_2}-dependence appears in high density regions. These results clearly demonstrate the scale dependence of the color-density relation. There exists a special scale where the environmental density affects galaxy colors the most. The value of this 'optimal adaptive smoothing scale' is $\sim 2h^{-1}$ Mpc for $M_r 20$, and varies somewhat from high to low density regions. Our detailed analysis show that the variation is from $\sim 1.5h^{-1}$ Mpc in high density regions to $\sim 2.5h^{-1}$ Mpc in low density regions, consistent with that shown in Figure 8 for the scale dependence of the color-density correlation coefficient.

Our further studies find that a better way to quantify the environmental effects on a galaxy is to use adaptive smoothing, for example distance to its n*th*-nearest neighbor, which takes into account the variations of the environmental density naturally. We have tested the distributions for the n*th*-nearest neighbor distances, where $n = 1, 2, 3, 4$ are considered. We notice that the distance to the 3*rd*-nearest neighbor for $M_r 20$ sample is peaked at $2h^{-1}$ Mpc with a range mainly between $\sim 1h^{-1}$ Mpc and $3h^{-1}$ Mpc, therefore it represents the 'peak scale' suitably and adaptively, and we propose it as the optimal adaptive smoothing scale
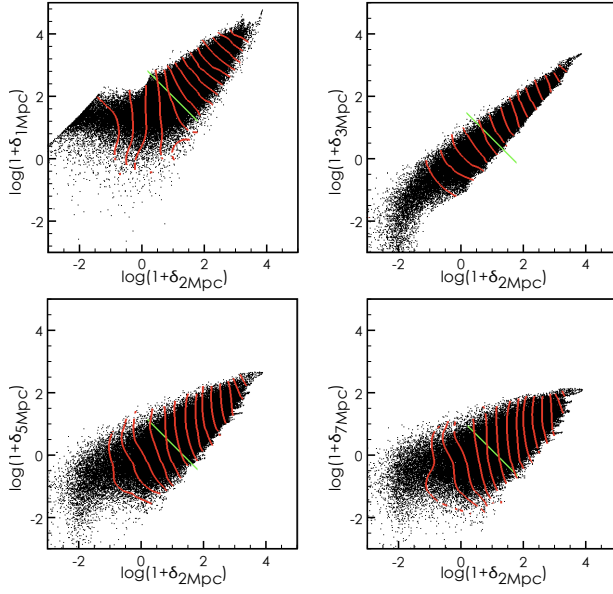
Figure A1. Scatter plots of $[\ln(1 + \delta_{R_1}), \ln(1 + \delta_{R_1})]$. In each panel, the red lines are galaxy color contours and the green line denotes the dividing line for high and low density regions.

for the $M_r 20$ sample. The corresponding optimal adaptive smoothing scales for the $M_r 19$ and $M_r 18$ samples are respectively 6th-nearest and 8th-nearest neighbors.